Coinage Metal Complexes with Di-tertiary-butyl Sulfide as Precursors with Ultra-Low Decomposition Temperature

Sweta Gahlot, Bhagyesh Purohit, Erwann Jeanneau, Shashank Mishra

Coinage Metal Complexes with Di-tertiary-butyl Sulfide as Precursors with Ultra-Low Decomposition Temperature

Sweta Gahlot,[a] Bhagyesh Purohit,[a] Erwann Jeanneau,[b] and Shashank Mishra*[a]

Abstract: We report here the synthesis of $[Cu_2(TFA)_4(^tBu_2S)_2]$ (**1**), $[Ag_4(TFA)_4(^tBu_2S)_4]$ (**2**) and $[AuCl(^tBu_2S)]$ (**3**) (TFA = trifluoroacetate), which decompose in solution medium at ultra-low temperature (e.g., in boiling toluene) to afford phase-pure and highly crystalline Cu_9S_5, Ag_2S and metallic Au nanoparticles, respectively. The low decomposition temperature of these precursors is attributed to the facile decomposition mechanism in the di-tertiary-butyl sulfide ligand. These results are a significant step in the direction of establishing a general low-temperature strategy spanning a range of systems including thermodynamically metastable materials and incorporate them in technologies that are sensitive to the harsh conditions.

The solution phase soft-chemical pathways to nanomaterials, such as sol-gel or metal-organic decomposition (MOD), have many advantages over traditional ceramic routes including access to desired forms of inorganic nanomaterials at much lower temperature.[1–5] These solution phase synthetic methods also provide a high homogeneity to the resulting chemical system, and are cost-effective and easy to implement at larger scale for the synthesis of nanomaterials.[6–8] As compared to the commonly used hydro/solvothermal synthesis, which usually results in the thermodynamically stable end products, the designed precursors with all the constituent elements pre-organized in a molecular framework can potentially influence the decomposition route and, consequently, overcome the thermodynamic impediments to produce nanomaterials under milder conditions and with better control over their properties, leading sometimes to isolation of even thermodynamically metastable phases. During molecule-to-materials transformation, the organic groups/ligands are eliminated to afford the desired metal-containing materials.[9,10] Therefore, a detailed understanding of the structural rearrangements and sequential elimination of the organic ligands during the transformation/degradation of these metal-organic precursors under certain reaction conditions is of utmost importance as it allows the rational design of specific compositions and morphologies of materials having improved chemical and electronic properties.[11] Since the 'hot injection' method reported in 1993 by Murray et al. for the synthesis of monodisperse cadmium chalcogenide nanoparticles (NPs),[12] several solution-phase methods involving either single source precursors or separate metal and chalcogenide reagents have been explored for the synthesis of colloidal metal chalcogenide NPs. These exploit a wide variety of different chalcogenide ligands/reagents such as tertiary phosphine chalcogenides, sulfur and selenium dissolved in octadecene or amines, chalcogenoureas, chalcogenolato, chalcogenocarbamato, xanthate, dichalcogeno-imidodiphosphinato, and so on.[13–15] However, a majority of these precursors require high temperature, a condition that not only enhance the grain growth but also favors formation of thermodynamically stable species only. General low-temperature synthetic strategies that span a range of systems are not yet well established. Lowering the reaction temperature requires identifying reagents that are reactive at low temperature. Other rationales behind exploring alternate chalcogenide reagents include low cost, ease of handling, non-toxicity, purity, and the ability to tune the nucleation and growth kinetics.

The silylated chalcogenoethers $(R_3Si)_2E$ (E = S, Se, Te) have been employed as excellent starting reagents for the synthesis of metal chalcogenide nanomaterials and clusters owing to their ability to transfer the chalcogenide anion (E^{2-}) under mild condition and versatility in reacting even with non-conventional metal reagents or being employed in a variety of synthetic methods.[16–18] These silylated chalcogenoethers react readily with a metal reagent MX_n (X = alkyl, halide, amide, carboxylate), where facile and homogeneous delivery of chalcogenide (E^{2-}) to the metal center and M–E bond formation are promoted by the generation and elimination of the corresponding R_3SiX.[19–23] On the contrary, the exploit of non-silylated chalcogenoethers R_2E (R = a non-silylated alkyl group; E = S, Se, Te) have been mainly restricted to the elaboration of thin films by chemical vapor deposition technique requiring usually high temperature.[24,25] Only recently, we have employed non-silylated selenoether ligands, particularly the ones having facile decomposition mechanism,[26] for the first time in the solution-phase synthesis of metal selenide NPs for the photocatalytic applications.[27–30] Thus, the reactions of $^tBu_2Se$ with coinage metal reagents not only resulted in the formation of binary and ternary metal selenide NPs at room temperature (RT) but also allowed us to isolate and characterize highly reactive molecular

[a] *Dr. S. Gahlot, Dr. B. Purohit, Dr. S. Mishra*
Université Lyon 1, CNRS, UMR 5256, IRCELYON
Institut de recherches sur la catalyse et l'environnement de Lyon
2 avenue Albert Einstein, 69626 Villeurbanne (France)
E-mail: shashank.mishra@ircelyon.univ-lyon1.fr

[b] *Dr. E. Jeanneau*
Université Lyon 1
Centre de Diffractométrie Henri Longchambon
5 rue de La Doua, 69100 Villeurbanne (France)

intermediates during the reactions. These have important implications in understanding the molecule-to-nanoparticle transformation better and developing a perspective for the synthesis of even compositionally complex materials with greater control.

Here we extend the above work to di-tertiary-butyl sulfide $^{t}Bu_2S$ by reasoning that C–S bond is more stable than C–Se bond, which should increase the stability of the intermediates sufficiently so that they become stable at RT but decompose at slightly higher temperature to generate metal sulfide NPs under ultra-mild but controlled conditions. Indeed, a lower reactivity of sulfide precursors in comparison to analogous selenide precursors has previously been demonstrated and explained on the basis of density functional theory (DFT) calculations.[31] As a case study, we focused our attention on coinage metals, as their chalcogenides offer numerous advantages such as low bandgaps, high chemical stability, high absorption coefficients, NIR surface plasmon oscillations, etc.,[32–34] and show a large variety of applications in the field of thermoelectrics,[35] photovoltaics,[36] bioimaging,[37] thermochromics,[38] and NIR absorption.[39]

The non-silylated di-tertiary-butyl chalcogenides, $^{t}Bu_2E$ (E = S, Se, Te) have been studied for their facile decomposition at low temperature, although their exact decomposition mechanism has been a subject of intense debate.[40,41] The possible initial steps in the decomposition include (i) C–E bond cleavage to give $^{t}Bu^{\bullet}$ and $^{t}BuE^{\bullet}$ radicals, and (ii) β –H elimination to give isobutene and tertiary-butyl chalcogenol (Scheme 1). While it was proposed using deuterium labelled experiments that $^{t}Bu_2Se$ undergoes decomposition *via* initial Se–C bond cleavage,[40] recently it was shown using ab initio calculations that the non-radical β-H elimination pathway could almost fully account for the decomposition of $^{t}Bu_2S$, even though radical reactions do have an effect on the product distribution.[31] This difference in the decomposition mechanism of $^{t}Bu_2Se$ and $^{t}Bu_2S$ may be traced to a slightly different bond strengths of the C–S and C–Se bonds, the former being thermodynamically more stable. Owing to this facile decomposition, the di-tertiary-butyl chalcogenides $^{t}Bu_2E$ (E = S, Se, Te) have been used as E-source in dual CVD to obtain thin films of metal chalcogenides.[42] However, this facile decomposition mechanism has been rarely exploited as a strategy in preparing single source precursors with low thermal decomposition temperature. In recent years, we have described direct synthesis of binary and ternary coinage metal selenide NPs $Cu_{2-x}Se$, Ag_2Se and AgCuSe at RT from the reaction of $^{t}Bu_2Se$ with $Cu(TFA)_2$ or/and Ag(TFA) (where TFA = trifluoroacetate) in a variety of solvents (diethyl ether, tetrahydrofuran or toluene).[27–30] Isolation and single crystal X-ray structural characterization of highly reactive intermediates $[Cu_2(TFA)_2(^{t}Bu_2Se)_3]$, $[Ag(TFA)(^{t}Bu_2Se)_2]$ and $[Ag_2Cu(TFA)_4(^{t}Bu_2Se)_4]$ during the course of these reactions confirmed that $Cu_{2-x}Se$, Ag_2Se and AgCuSe NPs are formed *via* above intermediates, respectively. These isolated intermediates are kinetically and/or thermodynamically unstable, as indicated by changes in their color within few days even at low temperature and in Argon atmosphere (they turn black due to their transformation into metal selenides) and confirmed by the DFT calculations.

Here we have extended these studies to $^{t}Bu_2S$. The rationale behind replacing $^{t}Bu_2Se$ with $^{t}Bu_2S$ was that a slightly stronger C–S bond in the later would enhance the stability of the intermediate at RT and ensure their decomposition only at slightly higher temperature. This would not only allow storage of the precursors at RT for longer period but also impart more control during their transformation to metal chalcogenide NPs. Indeed, $^{t}Bu_2S$ reacted differently with $Cu(TFA)_2$, Ag(TFA) or $HAuCL_4$ in toluene and, unlike reactions of $^{t}Bu_2Se$, did not lead to change in the color of the solutions or any precipitation even after stirring for 2–3 h at room temperature. However, upon refluxing, it yielded either black (in the cases of Cu and Ag) or brown (Au) precipitates immediately. While the XRD analysis of the black precipitate obtained from the reaction of $Cu(TFA)_2$ showed the presence of a mixture of Cu_9S_5 (ICDD #00-047-1748) and CuS (ICDD #00-006-0464, 22%) as the major and minor

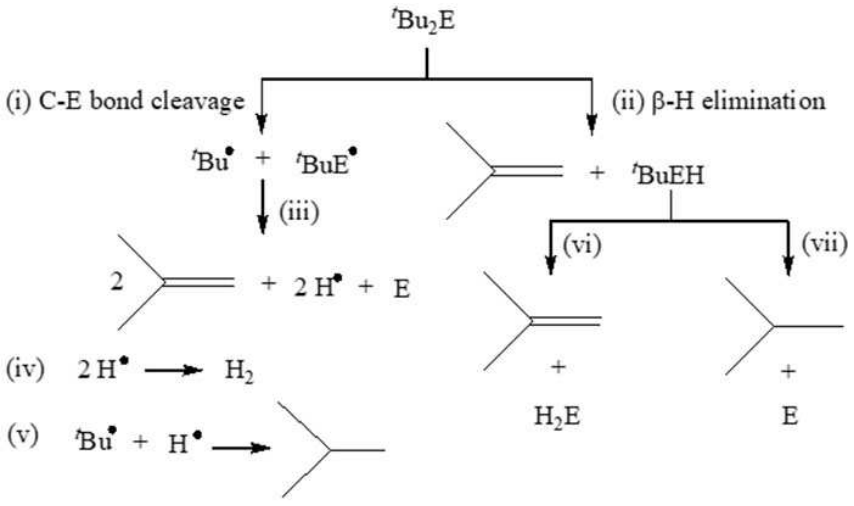

Scheme 1. The possible decomposition pathways of $^{t}Bu_2E$ (E = S, Se).

phases, respectively, the powder XRD of the precipitate obtained from the reaction with Ag(TFA) confirmed it to be single-phase Ag_2S (ICDD #00-014-0072) (Figure S1). The average crystallite size of the Ag_2S NPs (~40 nm), calculated using Debye-Scherrer equation, was found to be almost double than that for the copper sulfide NPs (~20 nm). The PXRD of the brown precipitate obtained from $HAuCl_4.H_2O$ showed it to be metallic gold (ICDD #00-004-0784).

To gain more insight on the above observations, we made attempts to isolate and identify the species present in the solutions before the precipitation of NPs. We succeeded in isolating crystalline molecular species $[Cu_2(TFA)_4(^tBu_2S)_2]$ (**1**) and $[Ag_4(TFA)_4(^tBu_2S)_4]$ (**2**) in good yield from the reactions of $^tBu_2S$ with trifluoroacetates of copper(II) and silver(I), respectively. In the case of reaction with $HAuCl_4.H_2O$, we isolated a Au(I) species $[AuCl(^tBu_2S)]$ (**3**) in good yield after two hours of stirring. On prolonged stirring (over 4 h), the initial Au(III) species is completely reduced to metallic gold nanoparticles (see below). The ability of chalcogenoethers to reduce metal centers has previously been demonstrated[31] and Au(III) thioether complexes have previously been shown to be reduced easily to Au(I) species by photo- or thermal-induced reductive elimination processes.[43] The FTIR spectra of **1**–**3** show characteristic bands for the ligand $^tBu_2S$, the copper and silver complexes also showing additional bands for the trifluoroacetate ligand (Figure S2). The ν_{as} (CO_2) appears at 1703 and 1670 cm^{-1} for **1** and **2**, respectively, indicating a bridging mode of coordination for the TFA group.[44] Expectedly, the ^1H NMR spectra of **2** and **3** in $CDCl_3$ showed a singlet at $\delta = 1.56$ and 1.60 ppm, respectively, for the ^{t}Bu group of the thioether.

The crystal structures of the molecular complexes **1**–**3** were determined using single crystal X-ray crystallography (Figure 1, Table S1). Complex $[Cu_2(\mu,\eta^1,\eta^1\text{-}TFA)_4(\eta^1\text{-}^tBu_2S)_2$ (**1**) crystallizes in monoclinic C2/c space group and adopts a discrete, paddle wheel dimeric structure, which is a commonly encountered structural motif among the copper carboxylate complexes.[45] All the trifluoroacetate ligands are in bridging μ,η^1,η^1-position with the Cu–O bond lengths lying in the range 1.935(5) to 2.087(5) Å (Table S2). A terminally bonded $^tBu_2S$ on each copper center (Ce–S = 2.479(2) Å) then completes a 5-coordinate environment for them, if a week Cu…Cu interaction (3.039(2) Å) is not taken into account. While the Cu–O bond distances compare well with the literature,[45] the Cu–S distance in **1** is actually shorter than those reported for related Cu(II) thioether complexes,[46] indicating that $^tBu_2S$ is strongly coordinated to copper center. The silver analogue $[Ag_4(\mu_3,\eta^1,\eta^2\text{-}TFA)_2(\mu,\eta^1,\eta^1\text{-}TFA)_2(\mu,\eta^1,\eta^1\text{-}^tBu_2S)(\eta^1\text{-}^tBu_2S)_3]$ (**2**), on the other hand, shows a zigzag tetranuclear structure constructed with the help of two triply bridging μ_3,η^1,η^2-TFA, two doubly bridging μ,η^1,η^1-TFA and one doubly bridging μ,η^1,η^1-$^tBu_2S$ ligands. The remaining three $^tBu_2S$ ligands are terminally bonded to Ag1, Ag3 and Ag4. While Ag1…Ag2 (2.999(6) Å) and A3…Ag4 (2.949(6) Å) have considerable argentophilic interaction, the distance between Ag2 and Ag3 is too long for such an interaction (3.636 Å).[47] The silver atom Ag1 (O_2S_2), Ag2 (O_3S) and Ag3 (O_3S) have a tetrahedral environment (if Ag…Ag interactions are not taken into account). The 3-coordinate Ag4, on the other hand, has O_2S

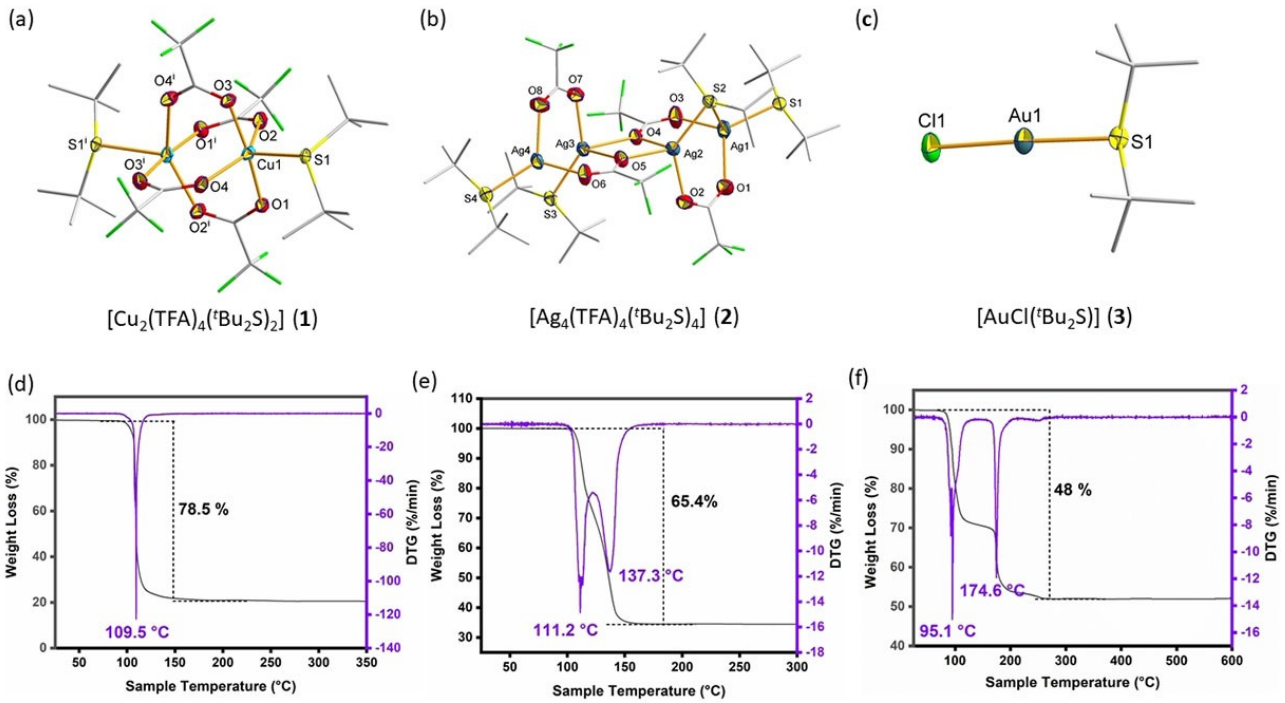

Figure 1. (a)–(c) Perspective view of the molecular structures of $[Cu_2(TFA)_4(^tBu_2S)_2]$ **1**, $[Ag_4(TFA)_4(^tBu_2S)_4]$ **2**, and $[AuCl(^tBu_2S)]$ **3** with 50% probability ellipsoids (H atoms omitted for clarity). (d)–(f) TGA (black) and DTG (blue) curves of **1**–**3**. Selected bond lengths (Å) and angles (°): (**1**): Cu1–O3 1.935(5), Cu1–O4 2.086(5), Cu1–S1 2.479(2), O1–Cu1–O2 87.6(2), S1–Cu1–O1 98.4(2). (**2**) Ag1–S1 2.496(1), Ag1–S2 2.793(2), Ag1–O3 2.298(5), Ag2–O2 2.244(5), S1–Ag1–S2 102.47(5), S1–Ag1–O1 114.2(1), O1–Ag1–O3 105.0(2). (**3**) Au1–S1 2.269(2), Au1–Cl1 2.263(2), S1–Au1–Cl1 176.48(9). Symmetry element, (**1**): (i) 1-x, +y, 1/2-z.

environment as the distance Ag4…S3 (3.190 Å) is significantly longer to be considered as a proper bond. The Ag–O distances range from 2.297(4) to 2.458(3) Å. The Ag–S distance for the bridging μ-^{t}Bu$_2$S group (2.789(1) Å) is longer than the corresponding η^1-^{t}Bu$_2$S ones (av. 2.446 Å) (Table S2). The monomeric complex [AuCl(^{t}Bu$_2$S)] (**3**) crystallizes in the monoclinic space group $P2_1/c$ and adopts the anticipated linear geometry at gold [S–Au–Cl 176.5(9)°]. The bond distances, 2.269(2) and 2.263(2) Å for Au–S and Au-Cl, respectively, compare well with those found in a related complex [AuCl(Me$_2$S)].[48] The discrete molecules of **3** are rather loosely packed in the crystal lattice and no extended aggregations are present (the shortest Au…Au contact is 6.220 Å) (Figure S3). The aurophilic interactions in Au(I) complexes, usually in the range of 2.9–3.6 Å, enhance the tendency for the molecules to aggregate within the crystal lattice and can lead to dimers, trimers, tetramers, or even polymeric networks that span throughout the solid state structure.[49]

The thermogravimetric studies of **1**–**3**, recorded under an argon atmosphere, confirmed their low thermal stability (Figure 1). The TG-DTG curves of the precursors **1** and **2** show that these are completely decomposed below 150 °C to afford metal sulfide. While **1** shows a sharp single step decomposition at 110 °C with a total weight loss of 79% (Figure 1d), the silver precursor **2** exhibits two distinct steps during decomposition (Figure 1e), as evident from two endothermic peaks at 111 and 137 °C in its DTG curve, and corresponds to a total weight loss of 65%. The residual weights for **1** (21%) and **2** (35%) are in agreement with the calculated weights for their complete conversion into Cu_9S_5 (19%) and Ag_2S (34%), respectively. Similar to **2**, the gold precursor **3** also shows a two-step decomposition in the temperature range 90–250 °C, which are accompanied by two DTG peaks observed at 95 °C and 174 °C (Figure 1f). A residual mass of 51.8% at 250 °C indicates the formation of gold as the end product (calculated value 52%). As described before, the low decomposition temperature of **1**–**3** can be attributed to the availability of a facile decomposition path in the ^{t}Bu$_2$S group.[40] To better understand the decomposition mechanism of this ligand, the gold complex **3**, which does not have any other organic group than the ^{t}Bu$_2$S group, was further studied by the TGA-mass spectrometry (TGA-MS). Evolution of isobutene, isobutane, and H_2S were observed as the major volatile products, the release time of the later lasting longer than the first two hydrocarbons. These major products are likely accounted for by the β-hydrogen elimination, releasing isobutene and isobutane and leaving sulfur on the surface, which along with Cl, are later released as H_2S and HCl, respectively. Thus, the first step in the TG-DTG curves, which corresponds to 30% mass loss, can be attributed to the loss of isobutene/isobutane molecules (theoretical value 29.6%). In the subsequent step, which accounts for 18% mass loss, Cl and S are probably lost simultaneously (theoretical value 17.8%) to afford gold NPs. To provide further support to this, we also synthesized silver trifluoroacetate complex with dimethyl sulfide ligand, for which there is no possibility of β-hydrogen elimination. The obtained complex of the composition [Ag(TFA)(Me$_2$S)] (**4**), as confirmed by elemental analysis and spectroscopic characterization, shows a single-step thermal decomposition in its TG-DTG curves that lasts well beyond 250 °C (Figure S4). The residual weight at 300 °C is 41.6%, which is in agreement with the theoretical value (43.7%) calculated for the formation of Ag_2S from two moles of **4**. Previously also, we have shown a relatively high decomposition temperature for the metal derivatives with Me$_2$E than those with ^{t}Bu$_2$E ligands (E = S, Se).[27,29,50]

The above observations indicated that **1** and **2**, which have direct metal-sulfur bonds as well as low thermal stability, would serve as excellent single source precursors (SSPs) for obtaining metal sulfide NPs at ultralow temperature. Therefore, we decomposed them in the presence of octadecanethiol (ODT) as a capping reagent using hot injection method. A solution of either **1** or **2** in a minimum amount of xylene was injected at once into a pre-heated solution of ODT-mixed xylene. On refluxing this mixture for an hour and then washing with ethanol and *n*-pentane, we recovered black precipitates of ODT-capped metal sulfide NPs in high yield, which were characterized by a range of physico-chemical analyses. The powder XRD of these NPs confirmed the presence of phase-pure *Digenite* Cu_9S_5 (ICDD #00-047-1748) and Ag_2S (ICDD #00-014-0072) with an average particle size of 10–12 nm (Figure 2a and 2e). The presence of octadecanethiol ligand around metal sulfide NPs was confirmed by FTIR and TGA studies. The FTIR spectra showed the characteristic bands for the ODT moiety at 2961, 2918 and 2848 cm^{-1} (Figure S5) which correspond to vibration modes of $\nu_{as}(CH_3)$, $\nu_{as}(CH_2)$ and $\nu_s(CH_2)$.[51] The TGA curves revealed that Cu_9S_5 and Ag_2S NPs contain about 6 and 21% by weight of octadecanethiol, respectively (Figure S6). This capping ligand starts to decompose at around 200 °C and is completely eliminated by 350 °C. Quantitative elemental analysis using EDX indicated high purity for these NPs (Figure S7). Further, TEM analyses (Figure 2b–d, Figure S8) show that Cu_9S_5 exists in the form of nano-dendrites and that the particle sizes are in the range of 5 to 15 nm. The high-resolution TEM (HR-TEM) images show lattice fringes for Cu_9S_5 with d-spacing of 0.33 nm (Figure S8b). The Fast Fourier Transform (FFT) analysis of the HR-TEM images further confirmed the presence of well-crystallized Cu_9S_5 (047-1748) (Figure 2d). The TEM analyses of Ag_2S NPs show that they have a spherical morphology with a uniform size distribution and an average particle size of 5 nm (Figure 2f and S9). The high-resolution TEM (HR-TEM) images show lattice fringes for Ag_2S with d-spacing of 0.23 nm (Figure 2g). The Fast Fourier Transform (FFT) analysis of this HR-TEM image further confirmed the presence of well crystalline silver sulfide (014-0072) (Figure 2h).

The XPS survey spectra of these ODT-capped Cu_9S_5 and Ag_2S NPs showed the presence of expected elements and the respective binding energies.[52–57] High-resolution core-level Cu 2p XPS spectrum for Cu_9S_5 NPs displayed two major peaks at binding energy 932 and 951.8 eV, for $2p_{3/2}$ and $2p_{1/2}$, respectively, which are characteristics of Cu^+ (Figure 3a).[52–54] This is further supported by the spin-orbit coupling spacing value ($2p_{3/2}$–$2p_{1/2}$) of 19.8 eV.[52] In addition, satellite peaks are observed at about 943 and 963 eV, which suggest the presence of some Cu^{2+} also. This is consistent with previous studies that have

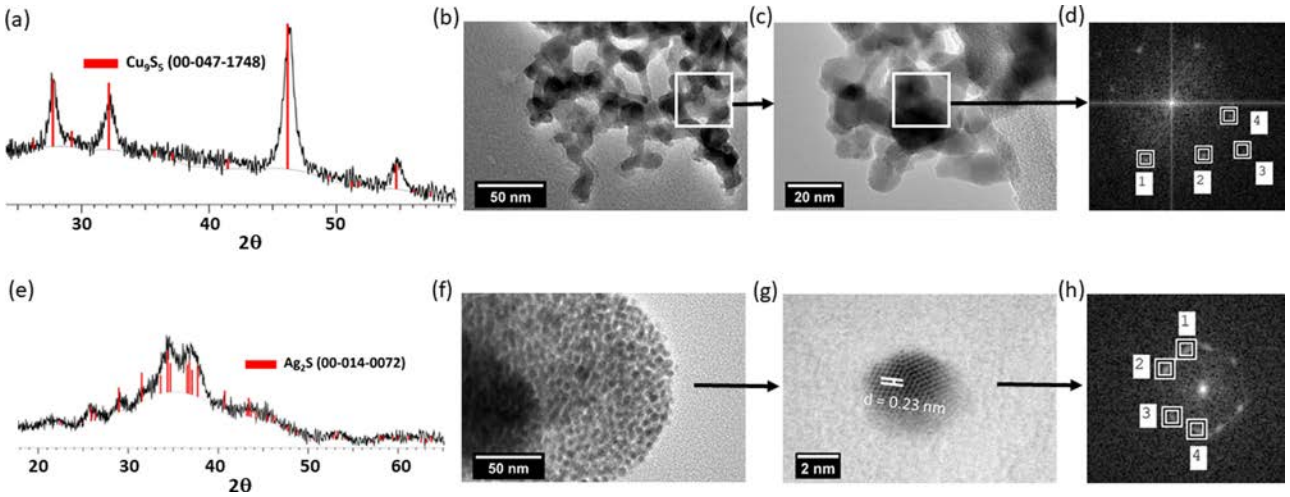

Figure 2. Characterization of octadecanethiol-capped Cu_9S_5 and Ag_2S nanoparticles prepared by using **1** and **2**, respectively, in hot injection method: (a)–(d) PXRD, TEM, HR-TEM and associated FFT of Cu_9S_5 NPs. The diffraction spots 1–4 in d) correspond to the plane {1 0 7}, {0 0 15}, {0 1 14} and {1 0 1}, respectively, of the ICDD #047-1748. (e)–(h), PXRD, TEM, HR-TEM and associated FFT of Ag_2S NPs. The diffraction spots 1–4 in h) are consistent with to the plane {-1 0 3}, {0 1 3}, {1 2 1}, and {1 1 2}, respectively, of the ICDD #014-0072.

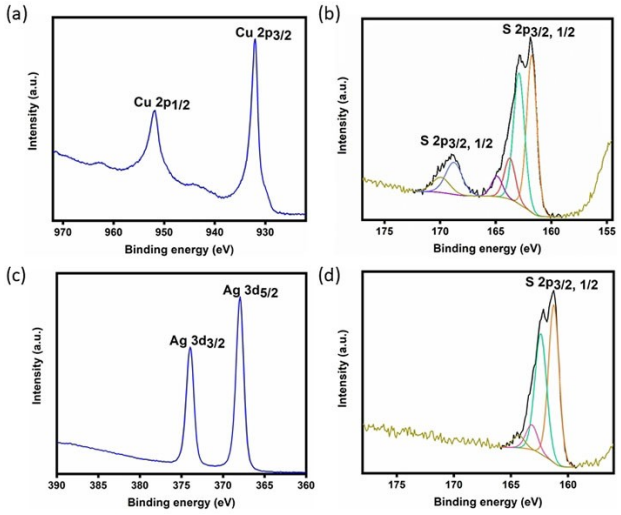

Figure 3. XPS spectra of of octadecanethiol-capped Cu_9S_5 and Ag_2S NPs showing binding energies of $Cu2p_{3/2}$ (a), $Ag3d_{5/2}$ (c) and Se3d (b and d).

shown the existence of both Cu^+ and Cu^{2+} in Cu_9S_5, the former being the major component.[52–54] The S 2p spectrum showed the $2p_{3/2}$ and $2p_{1/2}$ binding energy at 161.8 and 162.9 eV, respectively, due to S^{2-} in the *Digenite* mineral.[52–54] It also displayed existence of the additional deconvoluted peaks due to organic sulfur of the surface ODT ligand; 163.7 and 164.9 eV due to -SH group, and 168.8 and 169.9 eV due to oxidized CSO_3H group (Figure 3b). The XPS spectra of Ag_2S NPs revealed binding energies for Ag 3d ($3d_{3/2}$ at 374 eV and $3d_{5/2}$ at 368 eV) and S 2p ($2p_{1/2}$ at 162.4 eV and $2p_{3/2}$ at 161.2 eV), which are consistent with the composition and expected oxidation states of the elements present (Figure 3c and 3d).[55–57] The deconvoluted peaks at 163.2 and 164.3 eV are due to -SH of the surface ODT ligand. In literature, there exist several studies for the preparation of copper and silver sulfide NPs.[58–66] These reports mainly use sulfur reagents such as ammonium thiosulfate,[60] 1-decanethiol,[61] 1-dodecanethiol,[59] ammonium diethyldithiocarbamate,[62] sodium sulfide nonahydrate,[63] or 8-mercaptooctanoic acid[58] in high reaction temperatures (180–240 °C) and use reducing reagents such as $NaBH_4$ and hydrazine.[61,63] Existing studies that use SSPs for the synthesis of silver and copper sulfide nanoparticles report high thermal decomposition temperatures ranging from 200–400 °C.[52, 64–66]

The formation of Au NPs during prolonged stirring of **3** (or a mixture of $HAuCl_4$ and $^tBu_2S$) in an organic solvent was confirmed by PXRD which showed the presence of the pure phase (ICDD #00-004-0784). EDX confirmed the presence of pure Au NPs with no traces of any contamination (Figure S10). TEM images expectedly revealed the presence of polydispersed NPs, since no surfactant was employed to control the shape and size distribution of the NPs. The high-resolution TEM images clearly showed lattice fringes indicating high crystallinity for these NPs. In the FFT analysis of these NPs, the spots 1 and 2 correspond to the {1 1 1} and {2 0 0} planes, respectively, which along with an interreticular spacing of 0.25 nm, confirm the presence of the cubic crystal structure of gold ($Fm\bar{3}m$, 225, ICDD #00-004-0784) (Figure 4c and d). Preliminary studies show that the complex **3** also undergoes facile reduction to afford metallic gold under a wide variety of other conditions as well (photolysis, thermolysis, sonolysis), which underlines its flexibility as a precursor to Au NPs.

For the sake of comparison, we also studied the reactions of above coinage metal reagents with the silylated counterpart $(Me_3Si)_2S$, which resulted in instant precipitation of nanoparticles. Thus, direct reactions of copper(II) and silver(I) trifluoroacetates with $(Me_3Si)_2S$, using Et_2O as a solvent at RT result in instant precipitation of CuS and Ag_2S NPs, respectively. Figures S11 and S12 show the XRD patterns for copper and silver sulfides, respectively, where the peaks correspond to the

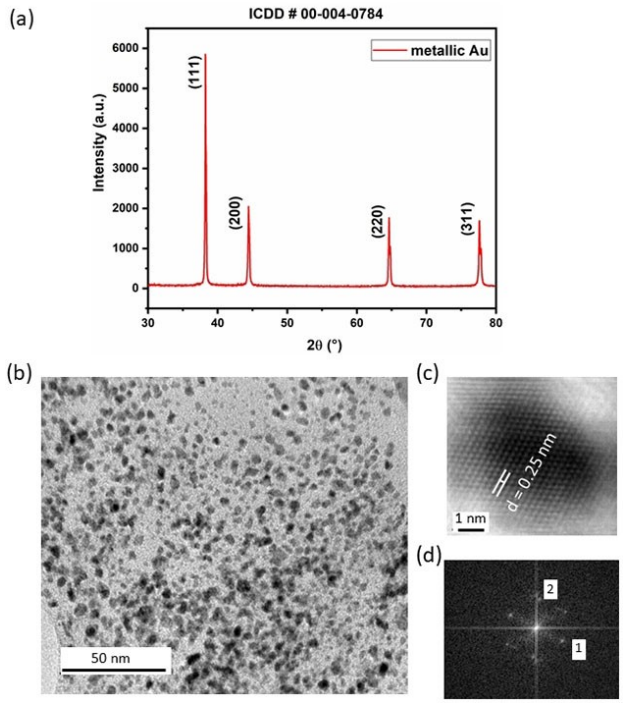

Figure 4. PXRD (a), TEM (b), HR-TEM (c) and associated FFT (d) of metallic Au NPs obtained from **3** at RT.

ICDD cards of 00-001-1281 for CuS and 00-014-0072 for Ag_2S. Similar reactions, when performed in the presence of octadecane thiol (ODT) as a capping ligand, resulted in instant formation of ODT-capped CuS and Ag_2S NPs (Figure S11 and S12). Powder XRD results showed the decrease in average particle size from 10 nm to 5 nm for CuS, and 45 nm to 30 nm for Ag_2S NPs due to the steric effect of the ODT ligand. The presence of ODT around these CuS and Ag_2S NPs were further confirmed by the FTIR spectra of ODT-capped NPs (Figure S13). Similar reaction with $HAuCl_4.H_2O$ in Et_2O at RT resulted in the formation of black precipitate, the XRD of which indicated it to be a poorly crystallized product (Figure S14). These observations underline the difference in the reactivities of the silylated and the non-silylated chalcogenoethers and, therefore, the mechanisms associated with them.

In summary, we exploit here the inherent facile decomposition mechanism in the $^tBu_2S$ ligand as a strategy to obtain molecular precursors with low decomposition temperature. These precursors, which are easily accessible through a simple synthetic protocol by using non-expensive commercially available reagents, decompose in solution phase at low- or even room temperature to afford phase-pure and highly crystalline Cu_9S_5, Ag_2S or metallic Au NPs. This strategy can easily be extended to a range of other systems including thermodynamically metastable or complex metal chalcogenide nanomaterials (ternary or multinary compositions in the form of particles, thin films or composites) with greater control.[67] The obtained metal sulfide NPs are currently being studied for photocatalytic applications.[27,28,30]

Experimental Section

General experimental procedures for the synthesis of the precursors **1**–**4** and their low temperature conversion to nanoparticles as well as X-ray crystallography are described in the Supporting Information.

Deposition Numbers 2079178 (for **1**), 2079179 (for **3**), and 2079180 (for **2**) contain the supplementary crystallographic data for this paper. These data are provided free of charge by the joint Cambridge Crystallographic Data Centre and Fachinformationszentrum Karlsruhe Access Structures service www.ccdc.cam.ac.uk/structures.

Acknowledgements

S.G. thanks the French ministry of higher education, research and innovation for her PhD grant (doctoral school of chemistry, Lyon). Authors also thank P. Bargiela (XPS) and Y. Aizac (PXRD) of IRCELYON and Dr. G. Ledoux of ILM (for access to TEM measurements).

Conflict of Interest

The authors declare no conflict of interest.

Keywords: chalcogenoethers · coinage metals · metal sulfides · molecular precursors · nanoparticles

[1] S. Mishra, S. Daniele, *Chem. Rev.* **2015**, *115*, 8379–8448.
[2] S. Mishra, S. Daniele, L. G. Hubert-Pfalzgraf, *Chem. Soc. Rev.* **2007**, *36*, 1770–1787.
[3] G. A. Seisenbaeva, V. G. Kessler, *Nanoscale* **2014**, *6*, 6229–6244.
[4] C. Panda, P. W. Menezes, M. Driess, *Angew. Chem. Int. Ed.* **2018**, *57*, 11130–11139; *Angew. Chem.* **2018**, *130*, 11298–11308.
[5] S. R. Alvarado, Y. Guo, T. P. A. Ruberu, E. Tavasoli, J. Vela, *Coord. Chem. Rev.* **2014**, *263–264*, 182–196.
[6] S. Mishra, S. Daniele, *Chem. Eur. J.* **2020**, *26*, 9292–9303.
[7] I. Bretos, R. Jimenez, J. Ricote, M. L. Calzada, *Chem. Soc. Rev.* **2018**, *47*, 291–308.
[8] C. Glynn, C. O'Dwyer, *Adv. Mater. Interfaces* **2017**, *4*, 1600610.
[9] a) L. G. Hubert-Pfalzgraf, *J. Mater. Chem.* **2004**, *14*, 3113–3123; b) M. Veith, *J. Chem. Soc. Dalton Trans.* **2002**, 2405–2412; c) H. Lu, D. S. Wright, S. D. Pike, *Chem. Commun.* **2020**, *56*, 854–871.
[10] a) A. B. S. Neto, M. G. A. Cruz, E. Jeanneau, A. C. Oliveira, N. Essayem, S. Mishra, *Dalton Trans.* **2021**, *50*, 1604–1609; b) B. Purohit, D. Amans, Y. Guyot, B. Mahler, M.-F. Joubert, C. Dujardin, S. Daniele, G. Ledoux, S. Mishra, *Mater. Today Chem.* **2020**, *17*, 100326; c) S. Mishra, E. Jeanneau, S. Daniele, V. Mendez, *Dalton Trans.* **2010**, *39*, 7440–7443.
[11] S. Mathur, M. Driess, *Comprehensive Organometallic Chemistry III*, (Eds.: R. H. Crabtree, D. M. P. Mingos), Elsevier, Oxford, **2007**, p. 35.
[12] C. B. Murray, D. J. Norris, M. G. Bawendi, *J. Am. Chem. Soc.* **1993**, *115*, 8706–8715.
[13] E. A. Weiss, *Acc. Chem. Res.* **2013**, *46*, 2607–2615.
[14] M. A. Malik, M. Afzaal, P. O'Brien, *Chem. Rev.* **2010**, *110*, 4417–4446.
[15] M. D. Khan, M. A. Malik, N. Revaprasadu, *Coord. Chem. Rev.* **2019**, *388*, 24–47.
[16] a) G. Shen, M. Chen, P. Guyot-Sionnest, *J. Phys. Chem. Lett.* **2017**, *8*, 2224–2228; b) H. Zhang, B. H. Savitzky, J. Yang, J. T. Newman, K. A. Perez, B. R. Hyun, L. F. Kourkoutis, T. Hanrath, F. W. Wise, *Chem. Mater.* **2016**, *28*, 127–134; c) B. Zhou, M. Li, Y. Wu, C. Yang, W. H. Zhang, C. Li, *Chem. Eur. J.* **2015**, *21*, 11143–11151.
[17] a) C. C. Lin, S. J. Tana, J. Vela, *J. Mater. Chem. A* **2017**, *5*, 20351–20358; b) A. Wolf, T. Hrtling, D. Hinrichs, D. Dorfs, *ChemPhysChem* **2016**, *17*, 717–723.

[18] E. E. Foos, R. M. Stroud, A. D. Berry, *Nano Lett.* **2001**, *1*, 693–695.
[19] K. T. Higa, K. A. Fallis, *J. Cluster Sci.* **2002**, *13*, 533–541.
[20] M. Gomez, C. Hernandez-Prieto, A. Martín, M. Mena, C. Santamaría, *Inorg. Chem.* **2016**, *55*, 3815–3821.
[21] J. P. Eußner, R. O. Kusche, S. Dehnen, *Chem. Eur. J.* **2015**, *21*, 12376–12388.
[22] G. Bendt, A. Weber, S. Heimann, W. Assenmacher, O. Prymak, S. Schulz, *Dalton Trans.* **2015**, *44*, 14272–14280.
[23] E. Dornsiepen, S. Dehnen, *Dalton Trans.* **2019**, *48*, 3671–3675.
[24] a) P. I. Kuznetsov, V. O. Yapaskurt, B. S. Shchamkhalova, V. D. Shcherbakov, G. G. Yakushcheva, V. A. Luzanova, V. A. Jitov, *J. Cryst. Growth* **2016**, *455*, 122–128; b) B. J. Choi, S. Choi, Y. C. Shin, K. M. Kim, C. S. Hwang, Y. J. Kim, Y. J. Son, S. K. Hong, *Chem. Mater.* **2007**, *19*, 4387–4389; c) N. D. Boscher, C. J. Carmalt, I. P. Parkin, *J. Mater. Chem.* **2006**, *16*, 122–127.
[25] a) S. L. Benjamin, C. H. Kees de Groot, C. Gurnani, S. L. Hawken, A. L. Hector, R. Huang, M. Jura, W. Levason, E. Reid, G. Reid, S. P. Richards, G. B. G. Stenning, *J. Mater. Chem. C* **2018**, *6*, 7734–7739; b) Y. Chang, A. L. Hector, W. Levason, G. Reid, J. Whittam, *Dalton Trans.* **2018**, *47*, 2406–2414; c) S. L. Benjamin, C. H. Kees de Groot, C Gurnani, A. L. Hector, R. Huang, E. Koukharenko, W. Levason, G. Reid, *J. Mater. Chem. A* **2014**, *2*, 4865–4869.
[26] D. J. Cole-Hamilton, *Chem. Commun.* **1999**, 759–765.
[27] S. Mishra, D. Du, E. Jeanneau, F. Dappozze, C. Guillard, J. Zhang, S. Daniele, *Chem. Asian J.* **2016**, *11*, 1658–1663.
[28] S. Gahlot, E. Jeanneau, F. Dappozze, C. Guillard, S. Mishra, *Dalton Trans.* **2018**, *47*, 8897–8905.
[29] S. Gahlot, E. Jeanneau, D. Singh, P. K. Panda, Y. K. Mishra, R. Ahuja, G. Ledoux, S. Mishra, *Inorg. Chem.* **2020**, *59*, 7727–7738.
[30] S. Gahlot, F. Dappozze, D. Singh, R. Ahuja, L. Cardenas, L. Burel, D. Amans, C. Guillard, S. Mishra, *Dalton Trans.* **2020**, *49*, 3580–3591.
[31] Y. Guo, S. R. Alvarado, J. D. Barclay, J. Vela, *ACS Nano* **2013**, *7*, 3616–3626.
[32] M. Dalmases, M. Ibanez, P. Torruella, V. Fernandez-Altable, L. Lopez-Conesa, D. Cadavid, L. Piveteau, M. Nachtegaal, J. Llorca, M. L. Ruiz-Gonzalez, S. Estrade, F. Peiro, M. V. Kovalenko, A. Cabot, A. Figuerola, *Chem. Mater.* **2016**, *28*, 7017–7028.
[33] R. Gui, H. Jin, Z. Wang, L. Tan, *Coord. Chem. Rev.* **2015**, *296*, 91–124.
[34] P. Reiss, M. Carriere, C. Lincheneau, L. Vaure, S. Tamang, *Chem. Rev.* **2016**, *116*, 10731–10819.
[35] M. Ferhat, J. Nagao, *J. Appl. Phys.* **2000**, *88*, 813–816.
[36] Y. Wu, C. Wadia, W. Ma, B. Sadtler, A. P. Alivisatos, *Nano Lett.* **2008**, *8*, 2551–2555.
[37] B. Dong, C. Li, G. Chen, Y. Zhang, Y. Zhang, M. Deng, Q. Wang, *Chem. Mater.* **2013**, *25*, 2503–2509.
[38] B. Gates, B. Mayers, Y. Wu, Y. Sun, B. Cattle, P. Yang, Y. Xia, *Adv. Funct. Mater.* **2002**, *12*, 679–686.
[39] G. Ku, M. Zhou, S. Song, Q. Huang, J. Hazle, C. Li, *ACS Nano* **2012**, *6*, 7489–7496.
[40] N. L. Pickett, D. F. Foster, N. Maung, D. J. Cole-Hamilton, *J. Mater. Chem.* **1999**, *9*, 3005–3014.
[41] C. A. Class, M. Liu, A. G. Vandeputte, W. H. Green, *Phys. Chem. Chem. Phys.* **2016**, *18*, 21651–21658.
[42] a) N. D. Boscher, C. J. Carmalt, I. P. Parkin, *Appl. Surf. Sci.* **2010**, *256*, 3178–3182; b) N. D. Boscher, C. S. Blackman, C. J. Carmalt, I. P. Parkin, A. G. Prieto, *Appl. Surf. Sci.* **2007**, *253*, 6041–6046; c) N. D. Boscher, C. J. Carmalt, I. P. Parkin, *Chem. Vap. Deposition* **2006**, *12*, 54–58; d) C. Thiandoume, O. Ka, A. Lusson, O. Gorochov, *J. Cryst. Growth* **1999**, *197*, 805–810.
[43] Z. Cao, D. M. Bassani, B. Bibal, *Chem. Eur. J.* **2018**, *24*, 18779–18787.
[44] S. Mishra, L. G. Hubert-Pfalzgraf, S. Daniele, M. Rolland, E. Jeanneau, B. Jouguet, *Inorg. Chem. Commun.* **2009**, *12*, 97–100.
[45] F. A. Cotton, E. V. Dikarev, M. A. Petrukhina, *Inorg. Chem.* **2000**, *39*, 6072–6079.
[46] J. M. Gonzalez-Perez, D. Choquesillo-Lazarte, A. Domínguez-Martín, E. Vílchez-Rodríguez, I. Pérez-Toro, A. Castiñeiras, O. K. Arriortua, M. E. Garcia-Rubiio, A. Matilla-Hernandez, J. Niclos-Gutierrez, *Inorg. Chim. Acta* **2016**, *452*, 258–267.
[47] H. Schmidbaur, A. Schier, *Angew. Chem. Int. Ed.* **2015**, *54*, 746–784; *Angew. Chem.* **2015**, *127*, 756–797.
[48] P. G. Jones, J. Lautner, *Acta Crystallogr.* **1988** *C44*, 2089–2091.
[49] K. M. Anderson, A. E. Goeta, J. W. Steed, *Inorg. Chem.* **2007**, *46*, 6444–6451.
[50] S. Mishra, E. Jeanneau, S. Daniele, *Polyhedron* **2010**, *29*, 500–506.
[51] D. Enders, A. Pucci, *Appl. Phys. Lett.* **2006**, *88*, 184104.
[52] B. Chakraborty, S. Kalra, R. Beltrán-Suito, C. Das, T. Hellmann, P. W. Menezes, M. Driess, *Chem. Asian J.* **2020**, *15*, 852–859.
[53] R. K. Sithole, L. F. E. Machogo, M. J. Moloto, S. S Gqoba, K. P. Mubiayi, J. V. Wyk, N. Moloto, *J. Photochem. Photobiol. A* **2020**, *397*, 112577.
[54] M. Hu, Z. Yu, J. Li, X. Jiang, J. Lai, X. Yang, M. Wang, L Sun, *RSC Adv.* **2017**, *7*, 38452–38457.
[55] H. Zhai, H. Wang, *Mater. Res. Bull.* **2008**, *43*, 2354–2360.
[56] W. Zhang, L. Zhang, Z. Hui, X. Zhang, Y. Qian, *Solid State Ionics* **2000**, *130*, 111–114.
[57] H. Lu, R. L. Brutchey, *Chem. Mater.* **2017**, *29*, 1396–1403.
[58] L. Kubie, L. A. King, M. E. Kern, J. R. Murphy, S. Kattel, Q. Yang, J. T. Stecher, W. D. Rice, B. A. Parkinson, *ACS Nano* **2017**, *11*, 8471–8477.
[59] L. Chen, G. Li, *ACS Appl. Mater. Interfaces* **2018**, *1*, 4587–4593.
[60] J. Kundu, D. Pradhan, *ACS Appl. Mater. Interfaces* **2014**, *6*, 1823–1834.
[61] D. Mott, J. Yin, M. Engelhard, R. Loukrakpam, P. Chang, G. Miller, I. Bae, N. C. Das, C. Wang, J. Luo, C. Zhong, *Chem. Mater.* **2010**, *22*, 261–271.
[62] F. Wang, Q. Li, L. Lin, H. Peng, Z. Liu, D. Xu, *J. Am. Chem. Soc.* **2015**, *137*, 12006–12012.
[63] I. O. Solorzano, M. Prieto, G. Mendoza, T. Alejo, S. Irusta, V. Sebastian, M. Arruebo, *ACS Appl. Mater. Interfaces* **2016**, *8*, 21545–21554.
[64] Y. Du, B. Xu, T. Fu, M. Cai, F. Li, Y. Zhang, Q. Wang, *J. Am. Chem. Soc.* **2010**, *132*, 1470–1471.
[65] Y. Wada, M. Kaneko, D. Niinobe, Y. Tsukahara, *Chem. Lett.* **2005**, *34*, 1618–1619.
[66] A. Sobhani, M. Salavati-Niasari, S. M. Hosseinpour-Mashkani, *J. Cluster Sci.* **2012**, *23*, 1143–1151.
[67] R. L. Brutchey, *Acc. Chem. Res.* **2015**, *48*, 2918–2926.